

A new approach to modelling friction stir welding using the CEL method

M. Hossfeld¹, E. Roos¹

¹Materials Testing Institute (MPA), University of Stuttgart
email max.hossfeld@mpa.uni-stuttgart.de

ABSTRACT

Although friction stir welding (FSW) has made its way to industrial application particularly in the last years, the FSW process, its influences and their strong interactions among themselves are still not thoroughly understood. This lack of understanding mainly arises from the adverse observability of the actual process with phenomena like material flow and deposition, large material deformations and thermomechanical interactions determining the mechanical properties of the weld.

To close this gap an appropriate numerical model validated by experiments may be helpful. But because of the issues mentioned above most numerical techniques are not capable of modelling the FSW process. Therefore in this study a Coupled Eulerian-Lagrangian (CEL) approach is used for modelling the whole FSW process. A coupled thermomechanical 3D FE model is developed with the CEL formulation given in the FE code ABAQUS® V6.12. Results for temperature fields, weld formation and the possibility of void formation are shown and validated.

KEYWORDS: FEM, friction stir welding, coupled eulerian lagrangian, microstructure, experimental validation

1. INTRODUCTION

Friction stir welding (FSW) is a solid-state joining process mostly used for the joining of aluminium alloys. Invented in 1991 at TWI in England [1, 2], FSW has made its way to industrial application particularly in the last years [3]. At first, this is because of the capability of producing welds with excellent properties like very good static and fatigue strength, low distortion and almost plain surfaces even in the as-welded condition [4, 5]. Furthermore, the possibility to join dissimilar materials such as aluminium and steel or aluminium and copper enables tailored blanks for lightweight designs or low resisting high current connections. But beside this there are other uprising advantages of FSW as in today's production environmental issues become more and more important. FSW consumes only about 2.5% of the energy of laser welding [6]. Also unlike other welding processes, FSW is free of toxic fumes and without the need for filler, gas shield or post weld heat treatment of the (usually almost plain) process zone. In addition high strength FSW welded joints enable automotive light weight constructions with a better material utilisation degree and decreased fuel consumption.

2. FRICTION STIR WELDING PROCESS

2.1. Operational principles, tool geometry, parameters and resulting microstructure

Even though the FSW process implies complex interactions between material properties and flow, heat transport and process forces, the basic operational principles are quite simple. The process mainly consists of a combination of frictional heating of the material and a stirring motion caused by a rotating tool. While friction and also plastic work dissipation heat, soften and plastify the material, the stirring motion mixes the material across the interface, resulting in a characteristic microstructure.

Tool geometry

Because all these aforesaid tasks have to be fulfilled by the FSW tool, tool geometry and material are always issues of permanent optimization [7–9]. The tool consists of a cylindrical shoulder and a protruding pin. The shoulder performs two main functions. First, the application of the bigger part of the process forces such as downward force and torque. Second, it prevents the plastified material from being pushed out of the actual processing zone under the shoulder. Therefore, the shoulder is mostly carried out concave. Particularly with respect to welding thin sheets, the shoulder additionally contributes notably to material intermixture. The main functions of the pin are both stirring of the material and an additional heating of the workpiece. Usually the pin is carried out as truncated cone or as a cylinder. For a better intermixture or for certain applications also other tool geometries are used, for instance other pin base geometries like squares or triangles, sometimes provided with flutes, threads etc. or shoulders with spiral threads.

FSW process

The FSW process can be divided into three essential phases (Fig. 1). First, the usually slightly tilted tool is *plunged* into a joint until the shoulder contacts surface of the material. After a short time of pre-heating, called *dwelling*, the rotating tool is moved along the joint line until the desired length is reached. In a last step the tool is removed from the weld. The remaining exit hole can be avoided through a retractable pin. For the sake of completeness it is mentioned at this point that the process is also capable of three-dimensional welds and also spot welds.

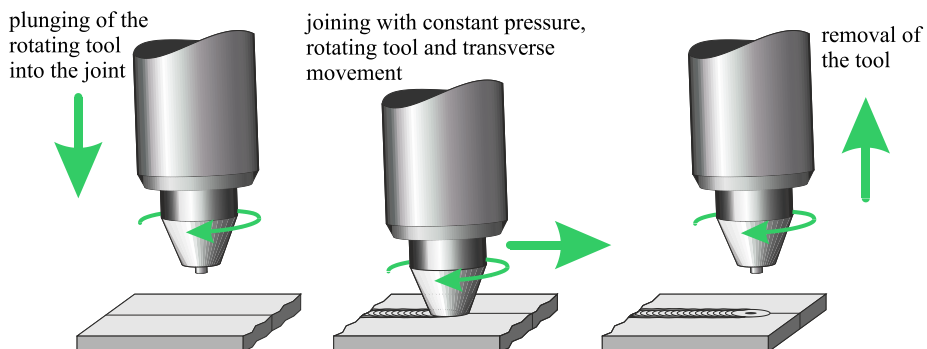


Fig. 1. The friction stir welding process. Illustrated without clamping.

Process parameters

The main process parameters of the friction stir welding process are rotational spindle speed ω , traverse speed V_x , tool angle α and downward force F_N (Fig. 2). The process may also be driven displacement-controlled. In this case the downward force F_N is a reaction of the depth of immersion. This depth is usually measured from the workpiece surface to the lowest part of the shoulder and called *heel plunge depth*.

It should be mentioned that not only the parameters determine important process factors such as generated heat, material transport or processing zone compression, but also they interact strongly. For instance a slightly increased angle of the tool may result in a significant increased downward reaction force in a displacement-controlled process.

By determining aforesaid process factors, the process parameters also determine directly the weld evolution and geometry, its microstructure, surface and the quality of the welded joint.

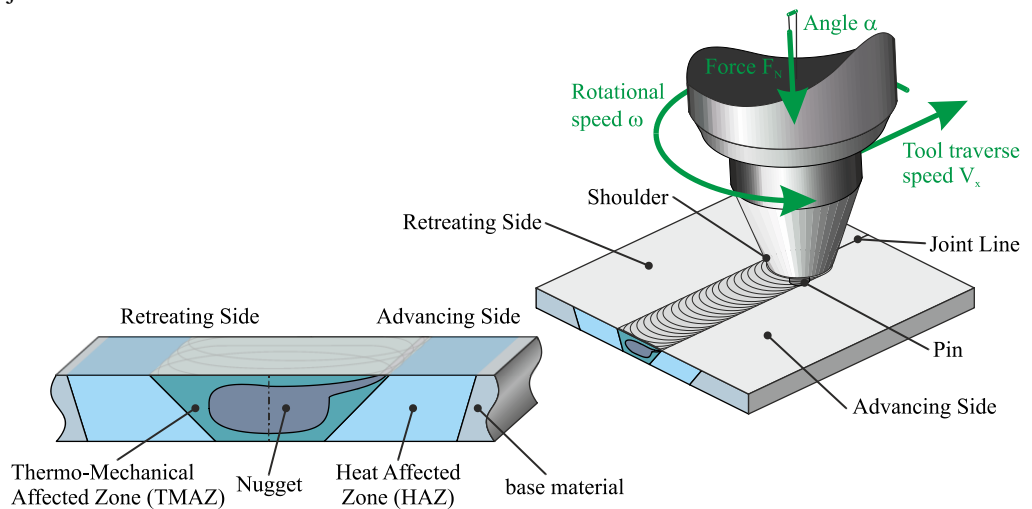


Fig. 2. Parameters of the friction stir welding process and microstructural zones.

2.2. Microstructure of friction stir welded joints

Friction stir welded joints consist of four characteristic zones showing different microstructure and so mechanical properties. These are

- An inner processing zone with very strong influences of pin and also shoulder, usually called **stirring zone** or **Nugget**
- A **Thermo-Mechanical Affected Zone (TMAZ)**
- The **Heat Affected Zone (HAZ)**, where influences of the temperature are observable
- The **base material** which is thermal and mechanical quasi unaffected

Figure 2 shows the different zones and their locations. In extreme cases, zones can grow or shrink significantly and almost merge together, e.g. when welding thin or very thick plates. Then a metallographic examination may not be as definite as in Fig. 3.

The shape of the **Nugget zone** depends remarkably on the tool geometry and the thickness of the plate. It is slightly unsymmetrical because of the tool rotation direction. Due to the severe solid state deformation during FSW this zone is fully dynamically recrystallized. This refines the grains up to diameters about 5-10 μm and thus results in a high-strength weld. This phenomenon is called Hall–Petch strengthening [10, 11].

The **TMAZ** surrounds the nugget zone on both sides. The **TMAZ** is also subjected to remarkable plastic deformation and heat input. In this zone the material is not stirred and not dynamic recrystallized, but the microstructure is usually heavily distorted and the affected grains are elongated, particularly at the transition to the nugget zone (Fig. 3). These elongated grains can reach easily lengths about 100 μm and widths about 5 μm . Furthermore, some recrystallization seeds can occasionally be found in the **TMAZ**.

The **TMAZ** in turn is enclosed by the **HAZ**. Although this zone is not subjected to plastic deformation the microstructure of the weld may be altered by the process heat input. Depending on the given aluminium alloy and its original condition this may range from slight grain growth to accelerated age hardening. For example a grain growth from ~35 μm to ~40 μm was observed in the **HAZ** for welded rolled AW 5182-0 sheets.

The influence of the microstructure on strength properties

As mentioned before, mechanical properties vary among the different zones. Beside the effects mentioned above, there are additional influences like coherent and incoherent dispersoids, generation of dislocations, misorientation of grain angles etc. [3, 12, 13]. Moreover, crack paths predefined for instance by oxide particles or dispersoids have definite effect on fatigue life [4, 14]. Crack growth rates are strongly driven by microstructure of the weld [15].

In summary, both the processing zone and the additional welding zones are stress concentrators as a consequence of material inhomogeneities.

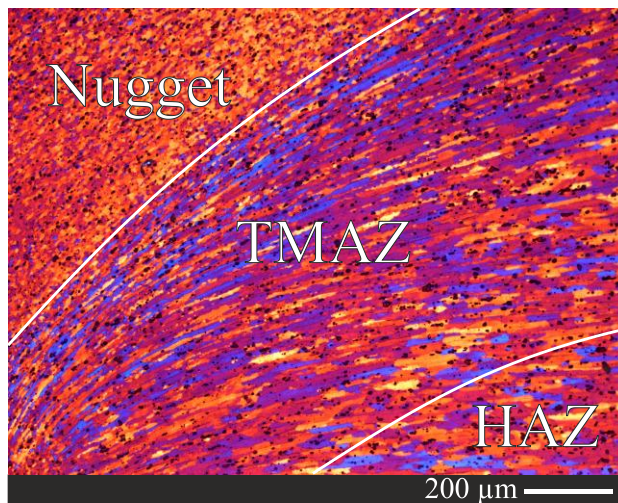


Fig. 3. Barker's etching on three characteristic microstructural zones of FSW.

3. NUMERICAL MODELING AND SIMULATION OF FSW

Although the basic principle of the process is simple, the modes of action in FSW are complex and not thoroughly understood. This lack of understanding mainly arises from the adverse observability of the actual process. To close this gap an appropriate numerical model validated by experiments may be helpful to investigate influences on the FSW process and their strong interactions. The challenging issues when modelling the FSW process are already contained in the process description above:

- large deformations and distortions
- mechanical properties of the materials are functions of temperature, strain, strain rate etc.
- non-linear phenomena like contact, friction etc.
- fluid-structure interaction
- detailed representation of the tool geometry if so with flutes, threads etc.
- representation of the weld geometry
- modelling the intermixture of the two sheets

Numerical models for FSW have been published by various authors, modelling techniques and goals [16–25]. Notable results were reached by use of the arbitrary Lagrangian–Eulerian formulation (ALE) by Ulysse [16], Schmidt and Hattel [17] or Guerdoux and Fourment [18]. When a lagrangian formulation is used, the main problem is the highly distorted mesh resulting in stability problems and time increment issues. Most authors deal with that by continuously remeshing or local mesh refinement, e.g. Guerdoux and Fourment [18]. In addition the *plunging* step of the FSW process is often not modelled because this easily causes excessive mesh distortion [17, 22]. Furthermore, very often only one instead of two sheets is used to represent the workpieces.

To avoid these issues, in this paper the Coupled Eulerian-Lagrangian (CEL) method by Noh [26] is investigated to model the FSW process. The CEL method uses a lagrange-plus-remap algorithm. When the mesh distorts during a lagrangian increment, the mesh is restored by calculating the material flow between elements and subsequent remapping [26, 27].

3.1. Numerical Model

The model was build up and simulated with the CEL formulation included in the FE code ABAQUS® Explicit V6.12 [27, 28]. The simulation represents all three phases of the FSW process shown in Fig. 1.

Geometry, assembly and boundary conditions

Figure 4 shows the assembly including boundary conditions. The tool is modelled as a linear-elastic lagrangian body. It has a length of 58 mm from which 35 mm belong to the fixture. The shoulder has a diameter of 12 mm with a concavity angle of 7°. The diameter of the pin is 5 mm and its length is 3 mm. The tool rotates with an angular speed of 209.5 rad/s while its tilt angle is 2°. The tool is represented in the model through 19,720 elements of type C3D8T. The two sheets lay within the eulerian mesh partial filled up with material. A gap between the sheets is possible for a more realistic setup (see Fig. 4 and Fig. 9). This feature may also be used for sensitivity analysis etc. The eulerian mesh with 255,300 elements of type EC3D8RT is bigger than the contained sheets. This enables the material flow and by this the

formation of the weld and burrs. When material passes over the borders of the eulerian mesh, the material and its properties are irretrievably lost.

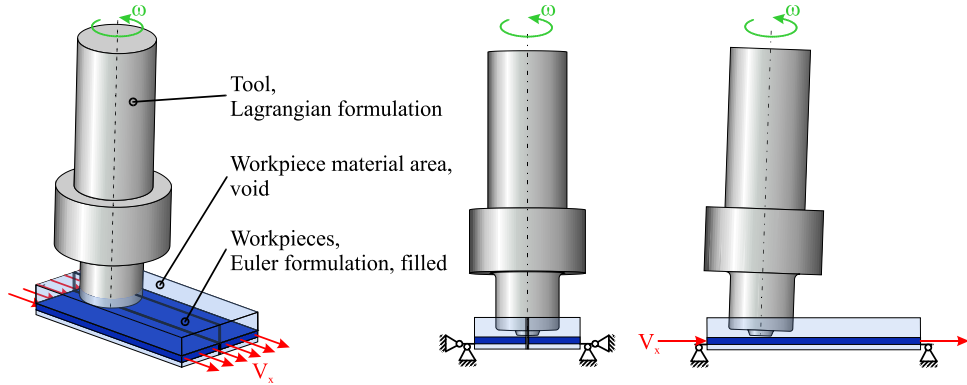


Fig. 4. Schematic model assembly. Illustrated without fixture and without tool shank.

The whole lower surfaces of the sheets are fixed in the z -direction. Also, all planes normal to the y -direction are fixed to avoid spreading. First, the rotating tool *plunges* into the two sheets ($V_z = 6 \text{ mm/s}$). After the subsequent *dwelling* phase planes normal to the x -direction are charged with a velocity ($V_x = 600 \text{ mm/min}$) to represent the feed motion. During the other phases, this velocity is set to zero. Heat dissipation from the welding process is modelled by heat conduction (tool shank and lower surface) and heat convection (upper surface and tool itself). These are given in Table 1 in the appendix. Furthermore, it is assumed that 100% of the friction dissipates in heat from which 90% flows into the aluminium sheet [29]. The environmental temperature is set to 20°C . The same thermal boundary conditions are used like in [18], see Table 2.

Material properties

The material parameters are extracted from literature and given in Tables 2 and 3 in the appendix. The elasticity of the aluminium alloy EN AW 6061 – T6 is modelled by an elastic–plastic Johnson–Cook [30] material model (1). Additional temperature dependent material parameters are given in Table 3. They are assumed to be isotropic.

$$\sigma_y = [A + B(\bar{\epsilon}^{pl})^n] \left[1 + C \ln \frac{\dot{\bar{\epsilon}}^{pl}}{\dot{\epsilon}_0} \right] \left[1 - \left(\frac{T - T_{ref}}{T_{melt} - T_{ref}} \right)^m \right] \quad (1)$$

Contact

The contact between tool and workpiece is represented by Coulomb’s law of friction with $\mu = 0.3$. A separation of tool and workpiece is possible. Schmidt and Hattel suggest this as a preliminary criterion for evaluating the success of the material deposition process during the simulation and important for a prediction when the suitable thermomechanical conditions and welding parameters are present [17].

In the model the contact was defined with the „ALL* with self“ contact algorithm. This algorithm determines the contact condition for every single node. When contact between nodes is detected friction, frictional heating etc. are respected.

4. RESULTS

Figure 5 shows the calculated temperature fields starting with the transient phases *plunging*, *dwelling* and the *transverse movement of the tool* until the process reaches the steady state. During *plunging* and *dwelling* burr formation behind the tool (*heel side*) are higher than in front because of the slightly tilted tool. For the same reason heat generation and temperatures are highest on the heel side of the tool.

Over the whole process the temperature field is almost symmetrical with a very slight asymmetry on the advancing side caused by the higher deposit of material in this area. This slightly higher burr formation on the advancing side during welding with transverse movement matches reality [4, 33] and is also shown in Fig. 8.

Furthermore, Fig. 5 shows that high temperatures are locally limited and the temperature gradient is very high in the welding direction. Both facts are plausible and are confirmed by metallographic examination (compare Fig. 3 and Fig. 6), own experiments and literature, e.g. [4, 17, 18, 33, 34]. Also shown is the development of a turning at the advancing side of the tool during welding. Although the simulated temperatures are high considering the material properties of AW 6061, they are in good accordance with the experimental temperatures of Assidi et al [34]. Further capabilities of the model are shown in Fig. 6–9. Figure 6 shows the calculated equivalent plastic strain, temperature and the result of metallographical examination. The relationship between temperature and plastic strain and microstructure evolution is obvious. For a better comparison the contour of *Nugget* and *TMAZ* is layed over the numerical results (white). The high magnitude of accumulated plastic strain matches the results of Assidi et al [34] as well as the elevated temperatures at pin tip and shoulder. As expected the CEL formulation is capable of handling these large deformations.

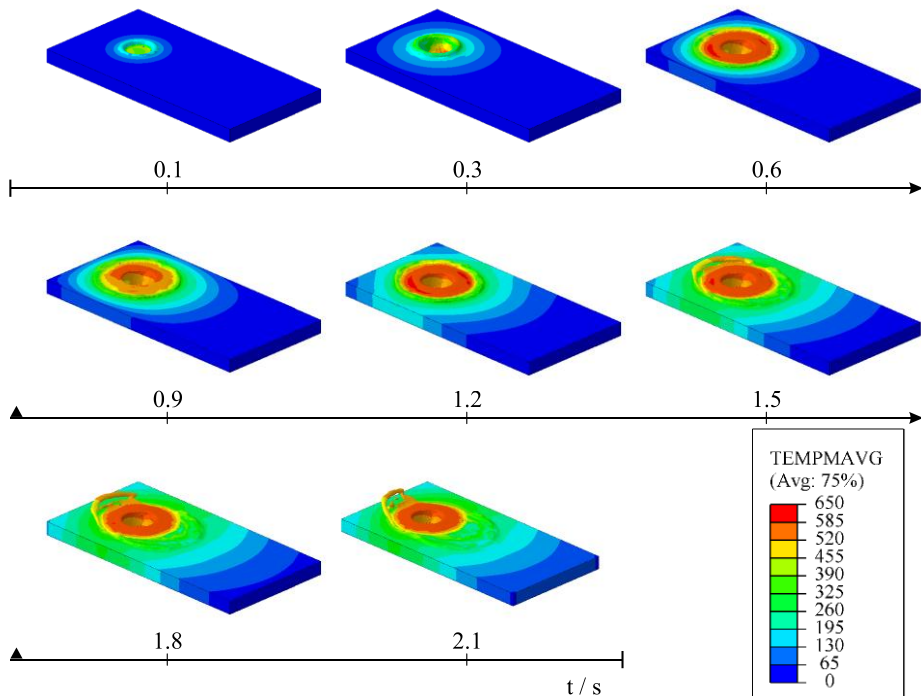


Fig.5. Timeline with calculated temperature fields and weld formation during the different phases of FSW. Tool and clamping are not shown. Temperature in degree Celsius.

Figure 7 shows a void formation at the bottom behind the tool due to failed material deposition. Moreover, Fig. 7 shows a metallographical examination of the appendant experiment. Figure 8 shows a stop action experiment with velocity vectors from the simulation with burr formation. These velocity vectors may enable a particle tracing for investigating the material flow during FSW. The possibility of a welding setup with a gap between the sheets is shown in Fig. 9.

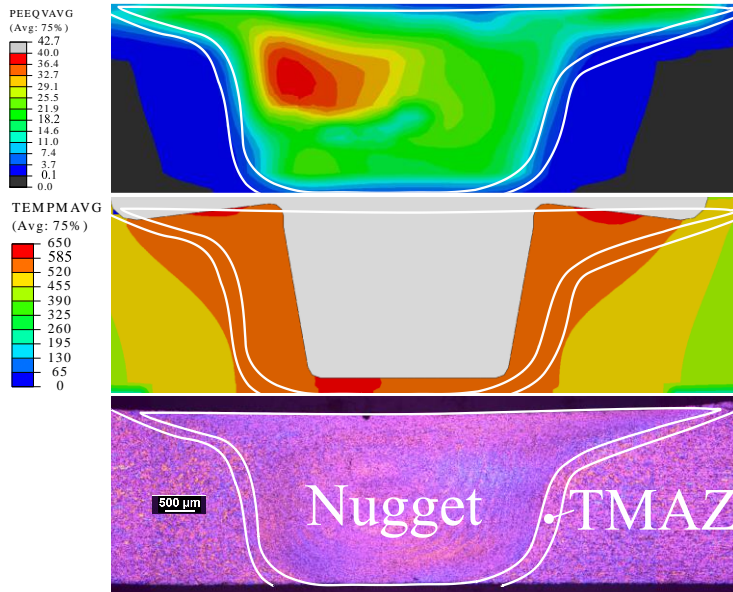


Fig. 6. Equivalent plastic strain, temperature and metallographical examination

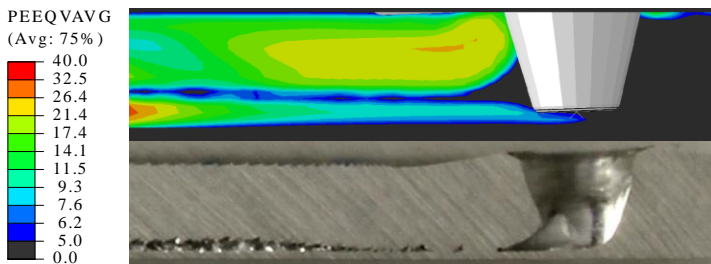


Fig.7. Void formation at the bottom behind the tool and metallographical examination.

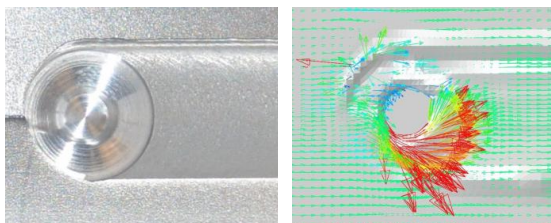


Fig. 8. Experimental stop action and velocity vectors of simulation

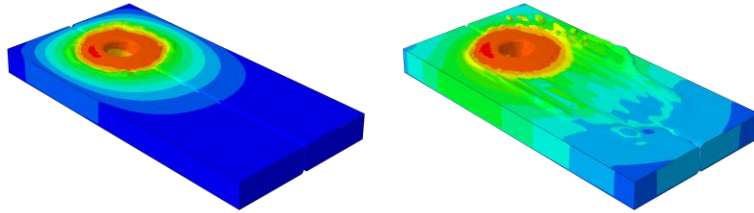


Fig. 9. Same setup as in Fig. 5 but with 0.3mm gap between the sheets

5. CONCLUSIONS

In this study the CEL method by Noh was used for modelling the FSW process. A fully coupled thermomechanical 3D FE model for the whole process was built up in ABAQUS® Explicit V6.12. Some numerical results were validated. The following conclusions can be drawn:

- The results of the FE model, especially temperatures, weld geometry and plastic strain are in good accordance with own experiments and literature.
- An estimation of the microstructure evolution seems possible by using the numerical results for temperature and plastic strain.
- Most of the presented requirements of modelling FSW and its phenomena can be met by CEL. Main advantages of the developed FE model are the capability of large deformations, material flow, the possibility of burr and void formation and free surface tracking respectively. Furthermore an improved set-up with two material sheets and intermixture is possible and was shown.
- A dense mesh is important for the sufficient tracking of free surfaces like burrs or the formation of voids. Material loss over the border of the eulerian region should be avoided because it may alter the results.
- The CEL formulation in ABAQUS® is capable of reaching the steady state within a relative short time. Even with a mesh dense enough to track free surfaces properly the calculation time is about 2 days on a 3,4 GHz Intel® i7 processor.
- By the use of the velocity vectors a particle tracking may be possible.
- Because Coulomb's law assumes that the frictional force is strictly proportional to the normal force and independent of the real contact area or the magnitude of the applied normal force [31] it has to be used with caution. To improve this friction law the use of a shear stress limit according to Orowan [32] may be applied. However it is not clear which stress limit is reasonable regarding influences like strain hardening etc.
- Like already mentioned by Guerdoux and Fourment [18] the simulation highly depends on appropriate constitutive and frictional models, while particularly the last is missing to this date for FSW. Non-linear friction phenomena like the influence of high pressure, velocity and temperature or even the influence of aluminium oxides require intense research. For example it is most likely that at the beginning of the FSW process friction is governed by aluminium oxide and that after a run-in period not only one shear layer determines friction.

ACKNOWLEDGEMENTS

The authors acknowledge support given by Deutsche Forschungsgemeinschaft (DFG) Project DFG RO 651/16-1.

APPENDIX

Table 1. Thermal boundary conditions of the model from [18].

Thermal exchange between	Tool	Backing plate	Tool shank	Ambient air (20°C)
Workpiece	50,000 W/m ² K	2,000 W/m ² K	-	30 W/m ² K
Tool	-	-	20,000 W/m ² K	20 W/m ² K
Backing plate	-	-	-	30 W/m ² K

Table 2. Johnson-Cook constants for AW 6061 – T6, from [35].

T_{melt} [°C]	A [MPa]	B [MPa]	C	N	m
582	293.4	121.26	0.002	0.23	1.34

Table 3. Temperature dependent material properties for AW 6061 – T6, from [23, 36].

Temperature	°C	37.8	93.3	148.9	204.4	260	315.6	371.1	426.7
Heat conductivity	W/mK	162	177	184	192	201	207	217	223
Specific heat	J/kgK	945	978	1004	1028	1052	1078	1104	1133
Density	g/cm³	2.685	2.685	2.667	2.657	2.657	2.630	2.630	2.602
Young's Modulus	GPa	68.54	66.19	63.09	59.16	53.99	47.48	40.34	31.72
Yield strength	MPa	274.4	264.6	248.2	218.6	159.7	66.2	34.5	17.9
Thermal expansion	10⁻⁶/K	23.45	24.61	25.67	26.60	27.56	28.53	29.57	30.71

REFERENCES

- [1] W.M. Thomas, E.D. Nicholas, J.C. Needham, M.G. Murch, P. Temple-Smith, C.J. Dawes, "Friction-stir butt welding", *GB Patent No. 9125978.8, International patent application No. PCT/GB92/02203*, 1991.
- [2] C.J. Dawes, W.M. Thomas, "Friction stir joining of aluminium alloys", *TWI Bulletin 6*, 1995.
- [3] F. Ostermann, "Anwendungstechnologie Aluminium," Berlin: Springer, 2007
- [4] Institut für Materialprüfung, Werkstoffkunde und Festigkeitslehre (IMWF) Universität Stuttgart, "Mikrostrukturorientierte Analyse des Ermüdungs- und Schädigungsverhaltens von FSW-Schweißverbindungen sowie Lebensdauervorhersage betriebsbeanspruchter FSW-Bauteile unter Berücksichtigung korrosiver Effekte", *Forschungsvorhaben AiF-Nr. 15685 N/4*, 2010.
- [5] A. Scialpi, M. de Giorgi, L.A.C. de Filippis, R. Nobile, F.W. Panella, "Mechanical analysis of ultra-thin friction stir welding joined sheets with dissimilar and similar materials", *Materials & Design*, Vol. 29, 2007, pp. 928–936.
- [6] R.S. Mishra, Z.Y. Ma, "Friction stir welding and processing", *Materials Science and Engineering*, Vol. 50, No. 1-2, 2005, pp. 1–78.
- [7] A. Arora, A. De, T. DebRoy, "Toward optimum friction stir welding tool shoulder diameter," *Scripta Materialia*, Vol. 64, 2011, pp. 9–12.
- [8] Y. Sakamoto, "Tool Development by Numerical Simulation," 8. *FSW Symposium*, Timmendorfer Strand, 2010.
- [9] K. Elangovan, V. Balasubramanian, "Influences of tool pin profile and tool shoulder diameter on the formation of friction stir processing zone in AA6061 aluminium alloy," *Materials and Design*, Vol. 29, 2008, pp. 362–373.
- [10] E.O. Hall, "The Deformation and Ageing of Mild Steel: III Discussion of Results", *Proceedings of the Physical Society London*, Vol. 64, No. 381, 1951, pp. 747–753.
- [11] N.J. Petch, "The Cleavage Strength of Polycrystals", *Journal of the Iron and Steel Institute*, Vol. 174, 1953, pp. 25–28.
- [12] ASM Handbook Volume 2: Properties and Selection: Nonferrous Alloys and Special-Purpose Materials, USA: ASM International, 1990.
- [13] D. Altenpohl, "Aluminium und Aluminiumlegierungen," *Reine und angewandte Metallkunde in Einzeldarstellungen*, Vol.19, Berlin-Göttingen-Heidelberg-New York: Springer, 1965.
- [14] M.N. James, D.G. Hattingh, G.R. Bradley, "Weld tool travel speed effects on fatigue life of friction stir welds in 5083 aluminium," *International Journal of Fatigue*, Vol. 25, 2003, pp. 1389–1398.
- [15] T.H. Tra, M. Okazaki, K. Suzuki, "Crack propagation microstructure Fatigue crack propagation behavior in friction stir welding of AA6063-T5: Roles of residual stress and microstructure", *International Journal of Fatigue*, Vol. 43, October 2012, pp. 23–29.
- [16] P. Ulysse, "Three-dimensional modeling of the friction stir-welding process", *International Journal of Machine Tools and Manufacture*, Vol. 42, 2002, pp. 1549–1557.
- [17] H. Schmidt, J. Hattel, "A local model for the thermomechanical conditions in friction stir welding", *Modelling and Simulation in Material Science and Engineering*, Vol. 13, 2005, pp. 77–93.
- [18] S. Guerdoux, L. Fourment, "A 3D numerical simulation of different phases of friction stir welding", *Modelling and Simulation in Material Science and Engineering*, Vol. 17, 2009, pp. 1–32.
- [19] B.C. Liechty, B.W. Webb, "Modeling the frictional boundary condition in friction stir welding," *International Journal of Materials Processing Technology*, Vol. 48, 2008, pp. 1474–1485.
- [20] A. Bastier, M.H. Maitournam, F. Roger, K. Dang Van, "Modelling of the residual state of friction stir welded plates," *Journal of Materials Processing Technology*, Vol. 200, 2008, pp. 25–37.

- [21] P.A. Colegrove, H. R. Shercliff, "3-Dimensional CFD modelling of flow round a threaded friction stir welding tool profile," *Journal of Materials Processing Technology*, Vol. 169, 2005, pp. 320–327.
- [22] M. Grujicic, T. He, G. Arakere, H. Yalavarthy, C. Yen, B. Cheeseman, "Fully coupled thermomechanical finite element analysis of material evolution during friction-stir welding of AA5083," *Proceedings of The Institution of Mechanical Engineers*, Vol. 224, 2010, pp. 609–625.
- [23] Y.J. Chao, X. Qi, "Thermal and Thermo-Mechanical Modeling of Friction Stir Welding of Aluminum Alloy 6061-T6," *Journal of Materials Processing and Manufacturing Science*, Vol. 7, 1998, pp. 215–233.
- [24] M. Awang, "Simulation of Friction Stir Spot Welding (FSSW) Process: Study of Friction Phenomena," College of Engineering and Mineral Resources at West Virginia University, Morgantown, West Virginia, 2007.
- [25] I. Alfaro, G. Racineux, A. Poitou, E. Cueto, F. Chinesta, "Numerical simulation of friction stir welding by natural element methods," *International Journal of Material Forming*, Vol. 2, 2009, pp. 225–234.
- [26] W.F. Noh, "CEL: A Time-Dependent, Two-Space-Dimensional, Coupled Eulerian-Lagrangian Code", *Methods in Computational Physics*, Vol. 3, 1964, pp. 117–179.
- [27] Modeling Extreme Deformation and Fluid Flow with Abaqus, Dassault Systèmes, 2012.
- [28] ABAQUS 6.12 Documentation, Dassault Systèmes, 2012.
- [29] T. Dickerson, Q. Shi, H. Shercliff, "Heat Flow Into Friction Stir Welding Tools," *Proceeding of the 4th International Symposium on Friction Stir Welding*, Park City, Utah, 2003.
- [30] G.R. Johnson, W. H. Cook, "A constitutive model and data for metals subjected to large strains, high strain rates and high temperatures", *Proceedings of the 7th International Symposium on Ballistics*, Vol. 21, The Hague, Netherlands: International Ballistics Committee, 1983.
- [31] P.J. Blau, "Friction science and technology. From concepts to applications", USA, FL, Boca Raton: CRC Press, 2009
- [32] E. Orowan, "The Calculation of Toll Pressure in Hot and Cold Flat Rolling", *Proceedings of Institutional Engineers Symposium*, Vol. 67, 1943, pp. 140–150.
- [33] Institut für Materialprüfung, Werkstoffkunde und Festigkeitslehre (IMWF) Universität Stuttgart, "Untersuchungen zur Übertragbarkeit der Prozessparameter auf Anlagen unterschiedlicher Bauart beim Herstellen von Tailored Blanks auf geschlossener Bahn mittels Rührreibschweißen", *Forschungsvorhaben AiF-Nr. 14572 N / DVS-Nr. 05.034*, 2007.
- [34] M. Assidi, L. Fourment, S. Guerdoux, T. Nelson, "Friction model for friction stir welding process simulation: Calibrations from welding experiments," *International Journal of Machine Tools and Manufacture*, Vol. 50, 2010, pp. 143–155.
- [35] A. H. Adibi-Sedeh, V. Madhavan, B. Bahr, "Extension of Oxley's analysis of machining to use different material models", *Journal of Manufacturing Science and Engineering*, Vol. 125, 2003, pp. 656–666.
- [36] J. Wong, P. Zambrano, M. P. Guerrero, V. Mucino, R. Colás, "Characterization of friction stir welding on aluminum," *Advanced Materials Research*, Vol. 68, 2009, pp. 167–174.